APPLIED SCIENCES AND ENGINEERING

Self-organization of maze-like structures via guided wrinkling

Hyung Jong Bae,[1] Sangwook Bae,[2,3] Jinsik Yoon,[4] Cheolheon Park,[4] Kibeom Kim,[4] Sunghoon Kwon,[1,2,3,5]* Wook Park[4]*

Sophisticated three-dimensional (3D) structures found in nature are self-organized by bottom-up natural processes. To artificially construct these complex systems, various bottom-up fabrication methods, designed to transform 2D structures into 3D structures, have been developed as alternatives to conventional top-down lithography processes. We present a different self-organization approach, where we construct microstructures with periodic and ordered, but with random architecture, like mazes. For this purpose, we transformed planar surfaces using wrinkling to directly use randomly generated ridges as maze walls. Highly regular maze structures, consisting of several tessellations with customized designs, were fabricated by precisely controlling wrinkling with the ridge-guiding structure, analogous to the creases in origami. The method presented here could have widespread applications in various material systems with multiple length scales.

INTRODUCTION

Two-dimensional (2D) to 3D transformation approaches, such as origami, kirigami, or mechanical instability, have attracted attention as alternatives to conventional lithography techniques for constructing complicated structures. Moreover, these self-organization methods can be applied to various functional material systems on different length scales (*1*). Consequently, they have been extensively studied for numerous applications, including functional machine fabrications (*2*, *3*), deformable energy storage devices (*4*), acoustic waveguides (*5*), optics (*6*), flexible devices (*7*), 3D electronics (*8*), and microfluidics (*9*), in addition to theoretical investigations (*10*–*16*).

As an interesting example of complex 3D structures, physical mazes have been useful tools for research purposes, such as maze solving (*17*, *18*) and the behavioral study of organisms (*19*, *20*), as well as providing a popular form of entertainment. However, the fabrication of these structures on microscales with designed directionality and uniformity but a chaotic architecture has been unexplored despite its potential applications. Among the self-organization techniques, wrinkling can be a potent approach to spontaneously construct maze-like structures, because the walls and pathways of the maze correspond to the ridges and valleys of the wrinkles, respectively. Moreover, the physical maze pathways can be organized with the randomness caused by the wrinkling, without using maze blueprints generated from the algorithms. Furthermore, wrinkling allows numerous identical structures to be simultaneously transformed into unique mazes.

However, owing to the intrinsic random nature of wrinkling, wrinkle control methods are necessary to satisfy the requirements for the maze structure. Since Bowden *et al.* (*21*) began fabricating aligned wrinkles on polydimethylsiloxane substrates, various control techniques have been developed, including prepatterning substrates or films (*22*–*24*), controlling stress states (*25*–*32*), and using molds (*33*). Although both parallel and perpendicular alignments of the ridges into prepatterned structures were achieved by changing the structural dimensions such as pitch and height (*22*, *23*), controlling the individual ridges to form in any direction was challenging because of the lack of elaborate control mechanisms. However, this type of ridge control is essential for various maze shape designs.

On the other hand, direct wrinkle patterning methods were developed using a focused ion beam (*34*) and lasers (*35*) for more precise patterning of wrinkles. Although these studies demonstrated the generation of wrinkles with designed patterns that were unachievable by the other methods discussed above, these techniques are inadequate for transformation purposes. This is because those approaches cannot fully use the advantages of the bottom-up nature of wrinkling, and thus, the self-organization of patterned structures with scalability is demanding.

Here, we have achieved a scalable self-organization of maze-like microstructures that had periodic patterns with specific directionalities while still using the bottom-up nature of wrinkling (Fig. 1A). To control intrinsically random wrinkles, we prepatterned ridge-guiding structures on the surface of the polymeric microparticle through photopolymerization of the prepolymer mixture by illuminating patterned and precisely focused ultraviolet (UV) light. Then, these prepatterned substrates were coated with silica for wrinkling (*36*). Using the guiding structures, we intended wrinkles to have directional order along the specific guided site. In addition, by using particle substrates, we provided isolated structures for complete individual mazes in the microscale and scalability in the structural design.

RESULTS

Guided wrinkling

The guiding structure consists of small grooves on one surface of the particle, which can only be geometrically transformed to valleys during the wrinkling process. That is, ridges can be generated only outside the grooves. By designing the arrangement of the grooves, we achieved precise control of ridge-guided sites and the corresponding wrinkle structure. For example, we fabricated a groove array with a checkerboard pattern on the particle surface by blocking UV light using 1 pixel–by–1 pixel black dots on the photomask (Fig. 1B). Then, the ridges had to be spatially ordered along either the horizontal or vertical direction because the ridge-guided site is restricted to those orthogonal lines by the guiding grooves. Although ridge orientation is directed in

[1]Nano Systems Institute, Seoul National University, Gwanak-ro, Gwanak-gu, Seoul 08826, South Korea. [2]Institute of Entrepreneurial Bio Convergence, Seoul National University, Gwanak-ro, Gwanak-gu, Seoul 08826, South Korea. [3]Interdisciplinary Program for Bioengineering, Seoul National University, Gwanak-ro, Gwanak-gu, Seoul 08826, South Korea. [4]Department of Electronics Engineering, Kyung Hee University, Deongyeong-daero, Giheung-gu, Yongin-si, Gyeonggi-do 17104, South Korea. [5]Department of Electrical and Computer Engineering, Seoul National University, Gwanak-ro, Gwanak-gu, Seoul 08826, South Korea.
*Corresponding author. Email: parkwook@khu.ac.kr (W.P.); skwon@snu.ac.kr (S.K.)

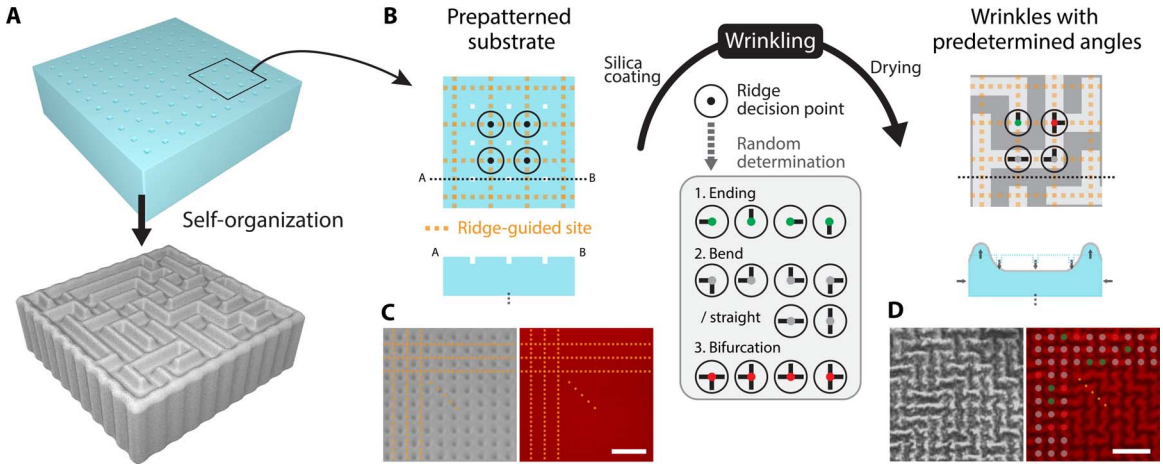

Fig. 1. Guided wrinkling for maze construction. (**A**) Self-organization of maze-like structures through wrinkling. (**B**) Schematic illustration of the fabrication process using ridge-guiding structures. First, the guiding structure composed of a groove array was prepatterned on the microparticle surface through the photopolymerization of the photocurable polymer with the corresponding photomask. Then, each ridge decision point was randomly transformed to either an ending, a bend, a straight line, or a bifurcation type during the wrinkling. According to the geometry of the ridge-guided site, wrinkles were spatially aligned in predetermined directions. (**C**) Bright-field and fluorescence image of the prepatterned substrate. The prepatterned microparticle immersed in ethanol was imaged by a CLSM. Dashed lines represent the ridge-guided site. Scale bar, 10 μm. (**D**) Bright-field and fluorescence image of the wrinkled microparticle. Each dot and its color in the fluorescence image represent a ridge decision point and its type shown in (B), respectively. Scale bar, 10 μm.

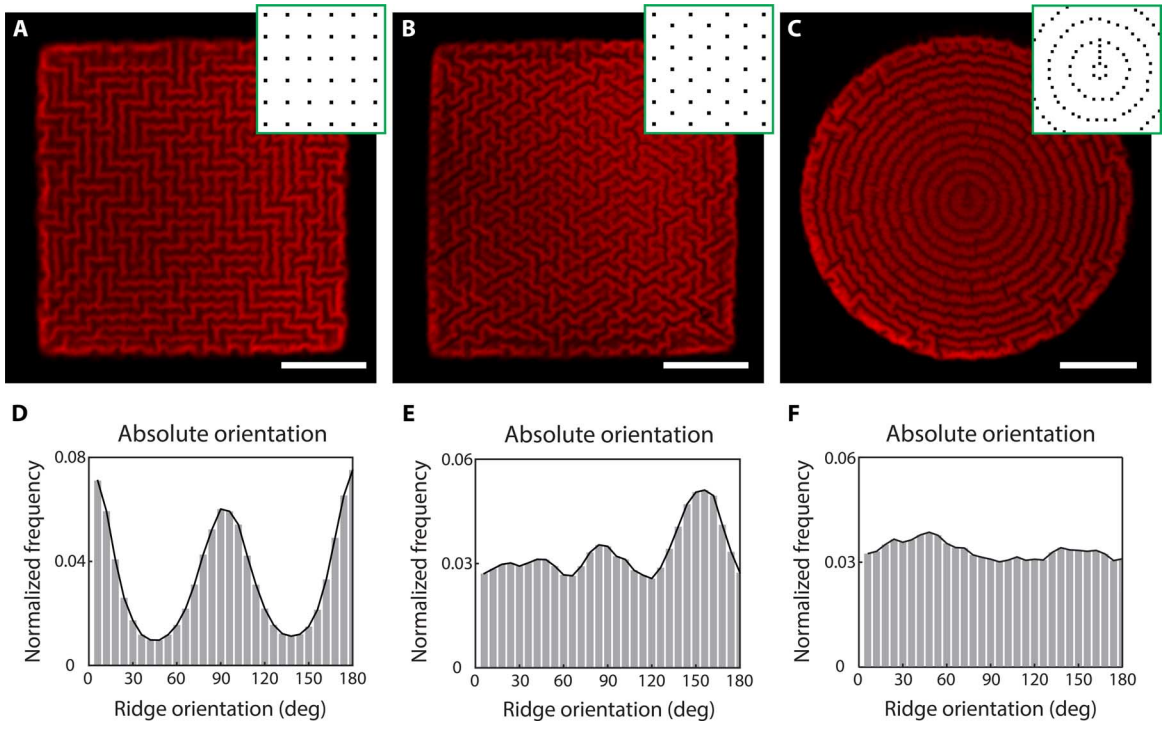

Fig. 2. Controlling maze tessellation. (**A** to **C**) CLSM images of the wrinkle patterns designed for orthogonal, sigma, and theta maze tessellations, respectively. The inset images show a part of the photomask for each pattern. Scale bars, 25 μm. (**D** to **F**) Distributions of the ridge orientation extracted from images with orthogonal, sigma, and theta tessellations, respectively. Each histogram contains ridge information from 20 microparticles.

predetermined angles, the type of ridge at each ridge decision point (the crossing point of two different ridge-guided lines) is randomly determined to either a ridge ending, a bend, a straight line, or a ridge bifurcation (see the Supplementary Materials and fig. S1 for the ridge organization). Consequently, the resulting microstructure showed maze-like topography, which exhibited a highly ordered but random network (fig. S2). Moreover, each transformed microstructure fabricated in the same batch had unique architecture while retaining programmed overall ridge orientations (fig. S3). We also found that the guiding structure itself could not show a specific pattern when scanned using a confocal laser scanning microscope (CLSM) (Fig. 1C). This reveals that the final structure was spontaneously organized through the wrinkling

process rather than through direct lithographical patterning (Fig. 1D). Overall, allowing both the control of ridge orientation and randomness of the ridge pattern is a distinctive feature compared to the previously developed self-organization methods using mechanical instability.

Control maze tessellation

Mazes have a variety of shapes, and they can be classified by tessellation, the configuration of a basic maze unit (*37*). To spontaneously construct physical mazes with specific tessellations, ridges should be precisely guided into their desired directions throughout the entire structure. We realized typical tessellations, which are orthogonal (maze unit formed into a perpendicular shape), sigma (maze unit formed into a hexagonal shape), and theta (ring-like shape), by prepatterning microparticles with appropriate groove array structures (Fig. 2, A to C). To qualitatively verify the accuracy of the tessellation controllability, we measured the orientation of the ridges from the CLSM image of microstructure samples in each tessellation group. The histogram of the ridge orientation distribution showed peak values at the corresponding programmed angles in the orthogonal and sigma shapes, and a relatively unbiased tendency in the theta shape, confirming that the ridges were well controlled on the basis of the guiding structure (Fig. 2, D to F). However, the sigma tessellation showed relatively unclear peaks when compared to the orthogonal tessellation. Observing the groove array structure for the sigma tessellation, we expected the ridges to be oriented at 0°, 60°, and 120° (fig. S4A). However, not all ridges were bent with those angles at the ridge decision points (fig. S4B). Specifically, when three or more ridge decision points were connected in one direction (diagonal or vertical directions), the angle orientation of the ridges tended to be tilted at 30°, 150°, or 90° orientations. The tilted angles of some ridges seem to have caused the peak values to be ambiguous.

Control the degree of ridge confinement

Further, some ridge patterns need to be preserved consistently in every structure for certain purposes (for example, partial variations of maze walls for distinct starting/ending sites), although overall patterns are unique. For this purpose, single ridges should be confined within the designed ridge-guided site. To achieve this, we first investigated the degree of ridge confinement along one axis by changing the dimension of the orthogonal groove array (Fig. 3A). The ratios of the distance between two grooves (d) to the characteristic wavelength (λ, the periodicity of the ridges in average) in both axes (d_x/λ and d_y/λ) were adjusted by designing photomasks while keeping particle synthesis and silica-coating conditions constant (see Materials and Methods and fig. S5). At the fixed value of d_x/λ, waves were well confined to the y axis when $d_y/\lambda \sim 0.25$, whereas kinked ridges to the x axis existed when $d_y/\lambda > 0.5$. When $d_x/\lambda = d_y/\lambda$ and each value ranged from 0.5 to 1, wrinkles were close to the orthogonal maze pattern. On the contrary, wrinkles were random when both values were greater than 1, or less than or equal to 0.25. When $d_x/\lambda \sim 2$, two wave lines were generated in the ridge-guided line.

Next, we extracted the constrained wavelength (λ') from the guided pattern and plotted λ'/λ according to d_x/λ to observe the guiding effect in terms of the wavelength (Fig. 3B). Here, we only examined $d_y/\lambda < 0.25$ cases to exclude the confinement of the straightness from consideration. When $d_x/\lambda < 0.4$ or $d_x/\lambda > 1.5$, the constrained wavelength was similar to the characteristic wavelength because the dimension of the guiding structure was too small or too large comparatively and thus had no confining effect. On the contrary, when d_x/λ ranged from 0.4 to 1.5, λ'/λ was proportional to d_x/λ, which verified that the wavelength of the guided patterns was controllable with the guiding structure dimensions in this range. However, when $1 < d_x/\lambda < 1.5$, the ridges showed a zigzag pattern rather than a straight one. This verified that the width of the individual ridges was not constrained in this range, although the overall periodicity was controlled because of the guiding grooves along the y axis.

Overall, single straight ridges can be confined within the ridge-guided line when the intergroove distance along the desired ridge

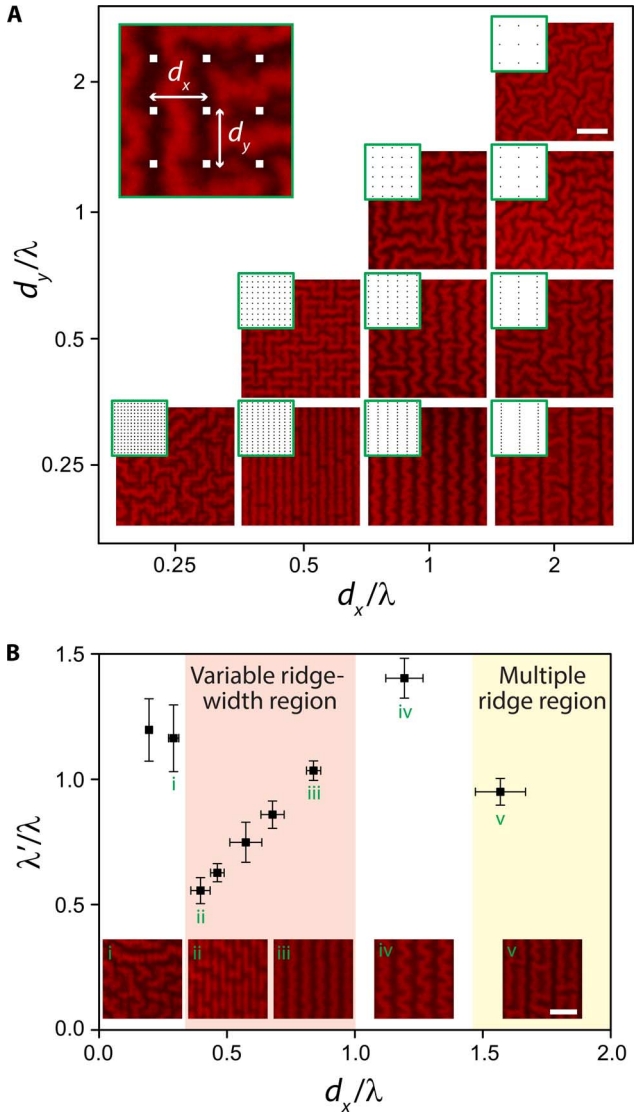

Fig. 3. Controlling the degree of ridge confinement along guiding structures. (**A**) Confinement of the ridge straightness based on the guiding structure dimensions. Photomasks for guiding structures were designed to satisfy several ratios between the characteristic wavelength (λ) and the dimensions of the ridge-guiding structure (d_x and d_y). The exact (d_x/λ, d_y/λ) values for the displayed CLSM images were (0.25, 0.25), (0.43, 0.22), (0.86, 0.22), (2.07, 0.26), (0.52, 0.52), (0.90, 0.45), (1.83, 0.46), (0.91, 0.91), (1.84, 0.92), and (1.83, 1.83) from the bottom left image, respectively. Scale bar, 10 μm. (**B**) Confinement of the pattern wavelength based on the guiding structure dimensions. The ratios between the characteristic wavelength and the constrained wavelength (λ') were extracted from the sample patterns guided with several d_x/λ values satisfying $d_y/\lambda < 0.25$. Error bars represented SDs, and $n = 7$ particles for each data point. Insets show representative patterns at the marked points. Scale bar, 10 μm.

direction is a quarter of the characteristic wavelength or less, whereas the width of the ridge-guided line is larger than 40% of the characteristic wavelength but smaller than the wavelength. That is, unidirectional wrinkles with any direction can be generated regardless of the characteristic wavelength of the pattern by designing the dimension of the groove array in a certain direction after determining the wavelength based on the UV light dose for the photopolymerization and the silica thickness. This highly uniform anisotropic pattern (fig. S6), as well as three different tessellation patterns presented, could be generated through the same isotropic shrinking process. This is a distinctive advantage over previous control methods, where the unidirectional patterning was usually possible by an anisotropic stress control by means of external guidance using mechanical devices, limiting heterogeneous pattern fabrication.

Demonstration of various mazes

Finally, using the developed delicate wrinkle control method, we demonstrated the construction of several physical mazes in microscale. First, we fabricated a general theta maze that had pathways start from the center and go to the outer edge of the structure (Fig. 4A). The boundary of the starting and ending points was fabricated by confining walls (ridges) along corresponding directions. In addition, we intentionally constructed straight pathways (valleys) from the ending region to the outside of the maze by prepatterning grooves on the desired sites. The fabricated mazes may have no solution path because the overall maze architecture is determined randomly during the wrinkling while the tessellation is controlled. Although the infeasibility of providing the solution path in every structure causes limitations, it seems advantageous for applications requiring scalability because constructing unique mazes or numerous maze-like structures is possible using one layout for a guiding structure.

Complex mazes, the three types of tessellations shown in Fig. 2, could be realized in a single structure by synthesizing prepatterned substrates using the combined photomask (Fig. 4B). Constructing heterogeneously controlled wrinkles in a single structure has been accomplished for the first time as far as we know. Some maze walls connected to each other in the boundary regions reveal that the complex maze structure was spontaneously generated on the microparticle during a single wrinkling process.

Furthermore, by generally applying ridge-confining rules over array structures, maze wall structures can be customized in a specific area while maintaining overall tessellations. For example, we inscribed letters with wrinkles by designing guiding structures to those letter shapes (fig. S7). The ridges of the letters were confined when the d/λ value of the guiding grooves was less than 0.25, which was consistent with the previous analysis. Using this mechanism, we successfully constructed letter-shaped walls inside the orthogonal maze (Fig. 4C). Overall, these highly versatile self-organizations originate from our novel wrinkle control method using ridge-guiding structures that can be simply prepatterned with any geometry. This transformation approach allows flexible and high-throughput fabrication of unique structures

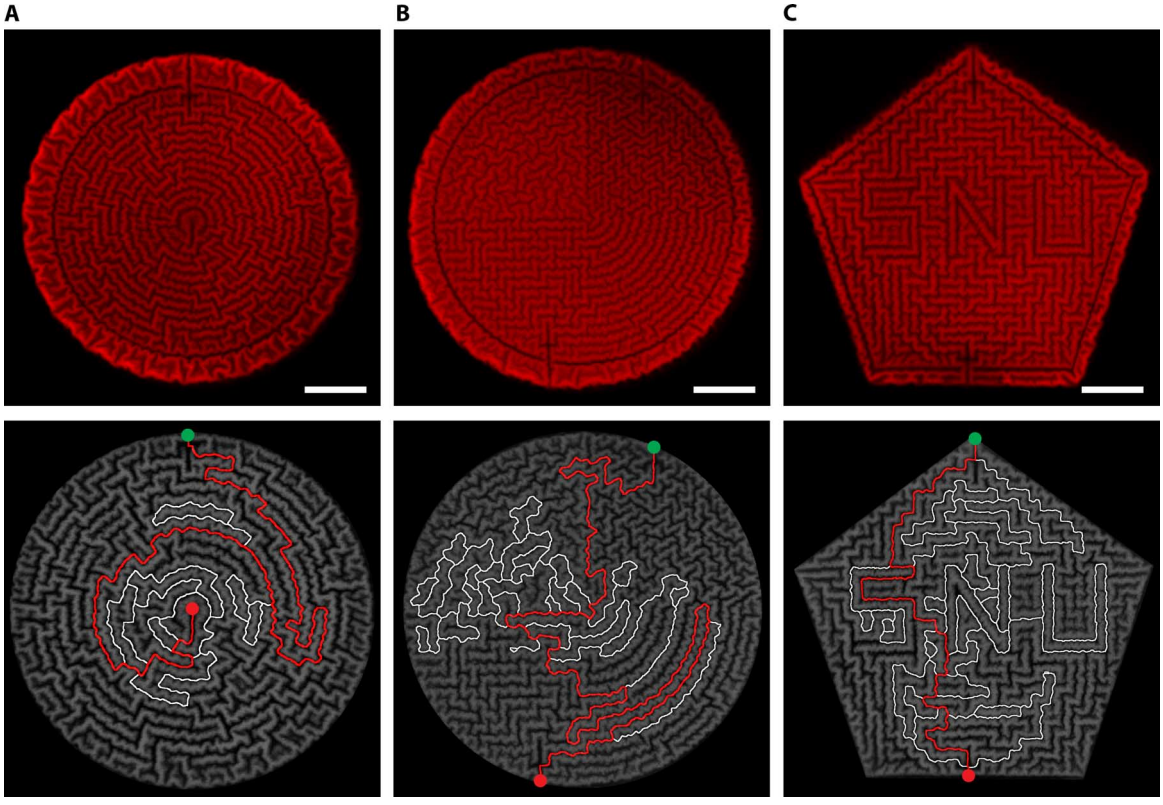

Fig. 4. Demonstration of various physical mazes. (**A**) Theta maze. Maze paths (lower image) were analyzed from the CLSM image (upper image). The starting point (red dot), the ending point (green dot), and the possible pathways (lines) are presented. The red line shows the shortest solution path. Scale bar, 25 μm. (**B**) Mixed maze. Wrinkles with four different directional orders (including random and anisotropic patterns) were generated in a single structure for a complex maze pattern. Scale bar, 25 μm. (**C**) Orthogonal maze containing a customized internal structure. Letter-shaped walls were fabricated in the middle of the maze without destroying the orthogonal maze pattern. Scale bar, 25 μm.

containing customized designs as well as periodic random architecture with different tessellations on a single substrate.

DISCUSSION

In summary, we have developed a wrinkling-based self-organization method for constructing physical mazes. By designing the arrangement of the groove arrays of the guiding structure, we allowed ridges with intrinsic disorder to have specific directionality. These precisely controlled ridges were used as the walls of mazes with different tessellations, including orthogonal, sigma, and theta shapes. In addition, we could generate these different tessellations on a single maze just by changing the photomask for the guiding structure. Furthermore, customization of the maze wall architecture was possible by confining single ridges inside the corresponding guiding structure with the appropriate design of d/λ values.

Ultimately, the resulting structures with highly periodic, ordered, but random architecture could have applications in various fields. First, one of their appealing uses is the generation of unique physical codes for security applications. In the field of security, hardware-based technologies have attracted significant attention because they provide powerful protection of secrete keys from hacking, compared to software-based technologies. As hacking skills improve, however, the hardware-based platforms will also be hacked and copied. As an alternative technology, physical unclonable functions (PUFs) have come into the spotlight recently. Because they generate private keys based on unclonable physical structures inhered in devices, it is hardly possible to extract the keys from the security system. Our unique maze structures with complex geometry could serve as PUFs for generating an unlimited number of private keys by integrating them into security chips. In addition, the developed self-organization method can be applied as a versatile encoding mechanism for microstructures, including authentication taggants. For example, if we use the distribution of minutiae points (ridge endings and bifurcations) as a code, the orthogonal maze patterns facilitate the classification of the encoded taggants based on the code complexity (fig. S8), allowing flexible code design according to the user's purposes. Moreover, the elaborate wrinkle control process provides smart code control mechanisms such as dual encoding (programmed graphical codes with random minutiae codes), enabling both a high information carrying capacity and a high security level. Besides these authentication purposes, the maze-like microstructures could be used as light-scattering layers in optics. For instance, the light extraction efficiency of the organic light-emitting diode can be improved by scattering light with these patterned structures. Furthermore, maze structures of various tessellations can be used as substrates for cell culturing, cell patterning, or studying the behavior of microorganisms in biological research. Although here we focused on the polymeric microparticle as the substrate, this sophisticated self-organization process can be generalized to various material systems at multiple scales for their given purposes.

MATERIALS AND METHODS

Materials

The photocurable prepolymer consisted of a 7:3 volume ratio of trimethylolpropane ethoxylate triacrylate (M_n ~ 428, Sigma-Aldrich) and 3-(trimethoxysilyl)propyl acrylate (Sigma-Aldrich) with a 10 volume % of Irgacure 1173 (BASF) as the photoinitiator to synthesize prepatterned microparticles functionalized for the silica coating. The 0.025 weight % of methacryloxyethyl thiocarbamoyl rhodamine B (Polysciences) was added to the prepolymer mixture for CLSM imaging of the surface wrinkle patterns. Ethyl alcohol anhydrous (99%; Daejung), ammonium hydroxide (25 to 28%; Daejung), deionized water, and tetraethyl orthosilicate (98%; Sigma-Aldrich) were used to coat the polymerized microparticle surface with silica.

Microparticle synthesis conditions

The power of the UV light shaped by the digital micromirror device was adjusted between 45 and 50 mW/cm^2 after passing through the 20× objective lens (numerical aperture, 0.45; Olympus). Then, this light was projected onto the prepared polymer resin for 150 to 200 ms. The UV power or curing time was tuned within the presented ranges to satisfy the appropriate characteristic wavelength of the wrinkle structure.

Analysis of the ridge orientation

We used a modified version of our previous fingerprint image-processing algorithm for the analysis (*36*, *38*). In brief, first, the confocal image of a wrinkled microparticle was transformed into gray scale. Then, within each image segment, we examined the local ridge orientations by calculating image gradients with simultaneous reliability checks. Ridge frequencies of the wrinkled particle were measured as the median frequency value across the whole image. The image then passed through an oriented image filter that used the ridge orientation and ridge frequency information to produce a ridge-enhanced image. Finally, the ridge orientations (represented as unit vectors with angles between 0° and 180° for each 3 pixel–by–3 pixel window) were extracted from the enhanced image. Ridge orientation histograms were plotted with a bin size of 6°.

Analysis of the degree of ridge confinement in guiding structures

To investigate the effect of the ratio of the distance between two grooves to the wavelength on the degree of ridge confinement, we separated the random and guided regions in every microparticle to extract the characteristic wavelength (λ) and the constrained wavelength (λ') with the guided pattern at the same time (fig. S5). We fixed the characteristic wavelength of samples by using the same UV light dose for the particle synthesis and silica-coating conditions within an experiment. The characteristic and constrained wavelengths were measured by fast Fourier transform analysis from the random and guided regions, respectively, of the CLSM images using ImageJ software. The distance between grooves (d) in both axes was controlled by changing the pixel distance between black dots in the photomask. The intergroove distance on the wrinkled surface (micrometers) was calculated using the microparticle size in the photomask (pixels), microparticle size in the CLSM image (micrometers), and interdot distance in the photomask (pixels). Then, both the d/λ and λ'/λ values were calculated for each microparticle sample.

Solving mazes

We used MATLAB to solve the fabricated mazes. First, we converted the original CLSM images of maze structures into binary images and inverted the colors so that black valleys in the CLSM image became white lines in the binary image. Then, we applied a thinning algorithm, "bwmorph" function with "skel" operation, to generate a binary skeleton image and specified the starting/ending points on this image. Next, we extracted possible pathways connecting the starting and ending points using the "bwlabel" function. Finally, the shortest pathway was searched by applying the "bwdistgeodesic" function.

SUPPLEMENTARY MATERIALS

Supplementary material for this article is available at http://advances.sciencemag.org/cgi/content/full/3/6/e1700071/DC1

fig. S1. Comparative analysis of the orthogonal ridge pattern in different generation methods.
fig. S2. Scanning electron microscopy image of a maze microparticle (scale bar, 10 μm).
fig. S3. Uniqueness of orthogonal patterns.
fig. S4. Ridge organization in a sigma tessellation.
fig. S5. Microparticle design for studying the guiding effect.
fig. S6. Controlling the anisotropic structure.
fig. S7. Inscribing letters with wrinkles.
fig. S8. Control of the code complexity.
movie S1. Generation of the guided wrinkles.

REFERENCES AND NOTES

1. S. H. Kang, M. D. Dickey, Patterning via self-organization and self-folding: Beyond conventional lithography. *MRS Bull.* **41**, 93–96 (2016).
2. S. Felton, M. Tolley, E. Demaine, D. Rus, R. Wood, A method for building self-folding machines. *Science* **345**, 644–646 (2014).
3. H.-W. Huang, M. S. Sakar, A. J. Petruska, S. Pané, B. J. Nelson, Soft micromachines with programmable motility and morphology. *Nat. Commun.* **7**, 12263 (2016).
4. Z. Song, T. Ma, R. Tang, Q. Cheng, X. Wang, D. Krishnaraju, R. Panat, C. K. Chan, H. Yu, H. Jiang, Origami lithium-ion batteries. *Nat. Commun.* **5**, 3140 (2014).
5. S. Babaee, J. T. B. Overvelde, E. R. Chen, V. Tournat, K. Bertoldi, Reconfigurable origami-inspired acoustic waveguides. *Sci. Adv.* **2**, e1601019 (2016).
6. L. Xu, X. Wang, Y. Kim, T. C. Shyu, J. Lyu, N. A. Kotov, Kirigami nanocomposites as wide-angle diffraction gratings. *ACS Nano* **10**, 6156–6162 (2016).
7. Y. Cho, J.-H. Shin, A. Costa, T. A. Kim, V. Kunin, J. Li, S. Y. Lee, S. Yang, H. N. Han, I.-S. Choi, D. J. Srolovitz, Engineering the shape and structure of materials by fractal cut. *Proc. Natl. Acad. Sci. U.S.A.* **111**, 17390–17395 (2014).
8. S. Xu, Z. Yan, K.-I. Jang, W. Huang, H. Fu, J. Kim, Z. Wei, M. Flavin, J. McCracken, R. Wang, A. Badea, Y. Liu, D. Xiao, G. Zhou, J. Lee, H. U. Chung, H. Cheng, W. Ren, A. Banks, X. Li, U. Paik, R. G. Nuzzo, Y. Huang, Y. Zhang, J. A. Rogers, Assembly of micro/nanomaterials into complex, three-dimensional architectures by compressive buckling. *Science* **347**, 154–159 (2015).
9. M. Jamal, A. M. Zarafshar, D. H. Gracias, Differentially photo-crosslinked polymers enable self-assembling microfluidics. *Nat. Commun.* **2**, 527 (2011).
10. J. L. Silverberg, J.-H. Na, A. A. Evans, B. Liu, T. C. Hull, C. D. Santangelo, R. J. Lang, R. C. Hayward, I. Cohen, Origami structures with a critical transition to bistability arising from hidden degrees of freedom. *Nat. Mater.* **14**, 389–393 (2015).
11. L. Mahadevan, S. Rica, Self-organized origami. *Science* **307**, 1740 (2005).
12. T. Castle, Y. Cho, X. Gong, E. Jung, D. M. Sussman, S. Yang, R. D. Kamien, Making the cut: Lattice *kirigami* rules. *Phys. Rev. Lett.* **113**, 245502 (2014).
13. T. Castle, D. M. Sussman, M. Tanis, R. D. Kamien, Additive lattice kirigami. *Sci. Adv.* **2**, e1601258 (2016).
14. E. Cerda, L. Mahadevan, Geometry and physics of wrinkling. *Phys. Rev. Lett.* **90**, 074302 (2003).
15. J. Yin, Z. Cao, C. Li, I. Sheinman, X. Chen, Stress-driven buckling patterns in spheroidal core/shell structures. *Proc. Natl. Acad. Sci. U.S.A.* **105**, 19132–19135 (2008).
16. X. Chen, J. Yin, Buckling patterns of thin films on curved compliant substrates with applications to morphogenesis and three-dimensional micro-fabrication. *Soft Matter* **6**, 5667–5680 (2010).
17. S. Mishra, P. Bande, *2008 IEEE International Conference on Signal Image Technology and Internet Based Systems (SITIS'08)*, Bali, Indonesia, 30 November to 3 December 2008.
18. M. J. Fuerstman, P. Deschatelets, R. Kane, A. Schwartz, P. J. A. Kenis, J. M. Deutch, G. M. Whitesides, Solving mazes using microfluidic networks. *Langmuir* **19**, 4714–4722 (2003).
19. T. Nakagaki, H. Yamada, A. Tóth, Intelligence: Maze-solving by an amoeboid organism. *Nature* **407**, 470 (2000).
20. J. Qin, A. R. Wheeler, Maze exploration and learning in *C. elegans*. *Lab Chip* **7**, 186–192 (2007).
21. N. Bowden, S. Brittain, A. G. Evans, J. W. Hutchinson, G. M. Whitesides, Spontaneous formation of ordered structures in thin films of metals supported on an elastomeric polymer. *Nature* **393**, 146–149 (1998).
22. C.-M. Chen, J. C. Reed, S. Yang, Guided wrinkling in swollen, pre-patterned photoresist thin films with a crosslinking gradient. *Soft Matter* **9**, 11007–11013 (2013).
23. W. T. S. Huck, N. Bowden, P. Onck, T. Pardoen, J. W. Hutchinson, G. M. Whitesides, Ordering of spontaneously formed buckles on planar surfaces. *Langmuir* **16**, 3497–3501 (2000).
24. E. P. Chan, A. J. Crosby, Fabricating microlens arrays by surface wrinkling. *Adv. Mater.* **18**, 3238–3242 (2006).
25. K. Efimenko, M. Rackaitis, E. Manias, A. Vaziri, L. Mahadevan, J. Genzer, Nested self-similar wrinkling patterns in skins. *Nat. Mater.* **4**, 293–297 (2005).
26. C.-C. Fu, A. Grimes, M. Long, C. G. L. Ferri, B. D. Rich, S. Ghosh, S. Ghosh, L. P. Lee, A. Gopinathan, M. Khine, Tunable nanowrinkles on shape memory polymer sheets. *Adv. Mater.* **21**, 4472–4476 (2009).
27. P.-C. Lin, S. Yang, Spontaneous formation of one-dimensional ripples in transit to highly ordered two-dimensional herringbone structures through sequential and unequal biaxial mechanical stretching. *Appl. Phys. Lett.* **90**, 241903 (2007).
28. D. Breid, A. J. Crosby, Effect of stress state on wrinkle morphology. *Soft Matter* **7**, 4490–4496 (2011).
29. P. Kim, M. Abkarian, H. A. Stone, Hierarchical folding of elastic membranes under biaxial compressive stress. *Nat. Mater.* **10**, 952–957 (2011).
30. E. Lee, M. Zhang, Y. Cho, Y. Cui, J. Van der Spiegel, N. Engheta, S. Yang, Tilted pillars on wrinkled elastomers as a reversibly tunable optical window. *Adv. Mater.* **26**, 4127–4133 (2014).
31. A. Chen, D. K. Lieu, L. Freschauf, V. Lew, H. Sharma, J. Wang, D. Nguyen, I. Karakikes, R. J. Hajjar, A. Gopinathan, E. Botvinick, C. C. Fowlkes, R. A. Li, M. Khine, Shrink-film configurable multiscale wrinkles for functional alignment of human embryonic stem cells and their cardiac derivatives. *Adv. Mater.* **23**, 5785–5791 (2011).
32. J. Yin, J. L. Yagüe, D. Eggenspieler, K. K. Gleason, M. C. Boyce, Deterministic order in surface micro-topologies through sequential wrinkling. *Adv. Mater.* **24**, 5441–5446 (2012).
33. P. J. Yoo, K. Y. Suh, S. Y. Park, H. H. Lee, Physical self-assembly of microstructures by anisotropic buckling. *Adv. Mater.* **14**, 1383–1387 (2002).
34. C. F. Guo, V. Nayyar, Z. Zhang, Y. Chen, J. Miao, R. Huang, Q. Liu, Path-guided wrinkling of nanoscale metal films. *Adv. Mater.* **24**, 3010–3014 (2012).
35. M.-W. Moon, S. H. Lee, J.-Y. Sun, K. H. Oh, A. Vaziri, J. W. Hutchinson, Wrinkled hard skins on polymers created by focused ion beam. *Proc. Natl. Acad. Sci. U.S.A.* **104**, 1130–1133 (2007).
36. H. J. Bae, S. Bae, C. Park, S. Han, J. Kim, L. N. Kim, K. Kim, S.-H. Song, W. Park, S. Kwon, Biomimetic microfingerprints for anti-counterfeiting strategies. *Adv. Mater.* **27**, 2083–2089 (2015).
37. M. Foltin, thesis, Masaryk University (2011).
38. Q. Xiao, H. Raafat, Fingerprint image postprocessing: A combined statistical and structural approach. *Pattern Recogn.* **24**, 985–992 (1991).

Acknowledgments

Funding: This work was supported by National Research Foundation of Korea grants funded by the Ministry of Science, ICT and Future Planning (nos. 2012-0009555, 2012M3A7A9671610, and 2015K1A4A3047345) and the Industrial Technology Innovation Program (10050991) funded by the Ministry of Trade, Industry and Energy (MI, Korea). This work was supported by a grant from Kyung Hee University in 2015 (KHU-20150514). **Author contributions:** W.P. and S.K. designed the experiments. H.J.B. conceived the ideas presented in the article and H.J.B., C.P., and K.K. developed the fabrication process. S.B. and J.Y. carried out the analysis of ridge patterns and maze pathways. **Competing interests:** The authors declare that they have no competing interests. **Data and materials availability:** All data needed to evaluate the conclusions in the paper are present in the paper and/or the Supplementary Materials. Additional data related to this paper may be requested from the authors.

Submitted 7 January 2017
Accepted 16 May 2017
Published 30 June 2017
10.1126/sciadv.1700071

Citation: H. J. Bae, S. Bae, J. Yoon, C. Park, K. Kim, S. Kwon, W. Park, Self-organization of maze-like structures via guided wrinkling. *Sci. Adv.* **3**, e1700071 (2017).

Self-organization of maze-like structures via guided wrinkling

Hyung Jong Bae, Sangwook Bae, Jinsik Yoon, Cheolheon Park, Kibeom Kim, Sunghoon Kwon and Wook Park

Sci Adv **3** (6), e1700071.
DOI: 10.1126/sciadv.1700071